

SCATTERING OUTCOMES OF CLOSE-IN PLANETS: CONSTRAINTS ON PLANET MIGRATION

CRISTOBAL PETROVICH¹, SCOTT TREMAINE², AND ROMAN RAFIKOV¹*Draft version April 22, 2014*

ABSTRACT

Many exoplanets in close-in orbits are observed to have relatively high eccentricities and large stellar obliquities. We explore the possibility that these result from planet-planet scattering by studying the dynamical outcomes from a large number of orbit integrations in systems with two and three gas-giant planets in close-in orbits ($0.05 \text{ AU} < a < 0.15 \text{ AU}$). We find that at these orbital separations, unstable systems starting with low eccentricities and mutual inclinations ($e \lesssim 0.1$, $i \lesssim 0.1$) generally lead to planet-planet collisions in which the collision product is a planet on a low-eccentricity, low-inclination orbit. This result is inconsistent with the observations. We conclude that eccentricity and inclination excitation from planet-planet scattering must precede migration of planets into short-period orbits. This result constrains theories of planet migration: the semi-major axis must shrink by 1-2 orders of magnitude without damping the eccentricity and inclination.

Subject headings: planetary systems – planets and satellites: dynamical evolution and stability – planets and satellites: formation

1. INTRODUCTION

Measurements of the orbital eccentricity and the projected misalignment between the spin of the host star and the orbit of extrasolar planets (i.e., the projected stellar obliquity ψ) have revealed that planetary architectures commonly differ from that of our own Solar System. The eccentricity distribution is broad, with $e > 0.3$ in $\sim 30\%$ of the planets, while the obliquity distribution (mostly from measurements of the Rossiter-McLaughlin effect from giant planets in close-in orbits) shows that $\sim 25\%$ of the planets have $\psi > 30^\circ$. Similarly, the existence of massive short-period planets—the so-called Hot Jupiters—points towards a dynamical history of known extrasolar planets that is quite different from that of the Solar System.

Different mechanisms have been proposed to account for the large eccentricities of giant planets: interaction with the natal protoplanetary disk (Goldreich & Sari 2003; Ogilvie & Lubow 2003), secular perturbations due to distant stellar (Wu & Murray 2003; Fabrycky & Tremaine 2007) or planetary companions (Naoz et al. 2011; Wu & Lithwick 2011), dynamical instabilities due to planet-planet gravitational interactions (Lin & Ida 1997; Rasio & Ford 1996; Weidenschilling & Marzari 1996), and others.

The mechanisms described above to excite the eccentricities that involve gravitational interactions with planetary or stellar companions can also potentially account for the observed high stellar obliquities and the presence of close-in planets, through tidal circularization of high-eccentricity, high-inclination orbits (e.g., Fabrycky & Tremaine 2007; Nagasawa et al. 2008). In contrast, gravitational interactions with the protoplanetary disk lead to migration and can account for the planets in close-in orbits, but are not expected to

produce large obliquities (e.g., Marzari & Nelson 2009; Kley & Nelson 2012).

Planet-planet gravitational interactions in multiple-planet systems have been extensively studied through N -body experiments and have been shown to reproduce the observed eccentricity distribution of planets with periods > 20 days reasonably well for a wide range of initial conditions (Ford & Rasio 2008; Jurić & Tremaine 2008; Chatterjee et al. 2008).

In this paper, we test a class of planet-formation models in which planets either migrate first or are formed at small orbital separations ($a \lesssim 0.2 \text{ AU}$) in low-eccentricity and low-inclination orbits ($e \lesssim 0.1$, $i \lesssim 0.1$), and then acquire their eccentricities and inclinations through planet-planet gravitational interactions. This situation could arise, for example, by means of disk migration without eccentricity and inclination excitation (or with eccentricity and inclination excitation which are subsequently damped) followed by disk dispersal, or through in-situ formation from a close-in disk resulting from a binary merger (Martin et al. 2011).

We recognize that our separation into two phases, “migration in the presence of gas”, and “planet-planet gravitational interactions without gas” is artificial and the planets might enter the gas-free phase in orbital configurations that differ from our assumed (nearly circular and coplanar) initial conditions (Libert & Tsiganis 2009; Lega et al. 2013). However, unless we make this separation it is hard to isolate the purely dynamical effects that take place after disk dispersal.

Two types of instability condition exist for systems containing a star and two or more orbiting planets. *Hill stability* requires that the planets preserve the ordering of the distances to the star, i.e., there are no orbit-crossing events. *Lagrange stability* requires both that the planets are Hill stable and that the outermost planet remains bound to the star (e.g., Barnes & Greenberg 2006). For two-planet systems, the former stability criterion has a well-defined boundary for the minimum separations of the planets with small eccentricities

¹ Department of Astrophysical Sciences, Princeton University, Ivy Lane, Princeton, NJ 08544, USA; cpetrovi@princeton.edu

² School of Natural Sciences, Institute for Advanced Study, Einstein Drive, Princeton, NJ 08540, USA

³ Taken from www.exoplanet.org as of November 2013.

(Gladman 1993), while the latter is less well-understood (Veras & Mustill 2013; Deck et al. 2013). Note that systems with more than two planets are not provably Hill stable for any initial separation (e.g., Chambers et al. 1996; Chatterjee et al. 2008).

Previous work by Ford et al. (2001) showed that the excitation of eccentricities and inclinations by gravitational interactions between planets (“planet-planet scattering”) is largely determined by the branching ratios into different dynamical outcomes such as planetary ejections, collisions with the star or planet-planet collisions. In particular, these authors show that simulations with two Jupiter-like planets placed initially in Hill unstable orbits result mostly in planet-planet collisions for the range of semi-major axes $0.5 - 2$ AU, and that the daughter planets produced in collisions have small eccentricities ($e < 0.05$). In contrast, planetary ejections leave the surviving planet with significant eccentricity: for two equal-mass-planet simulations Ford et al. (2001) find $e \sim 0.4 - 0.8$ for the survivor. Similar experiments by Ford et al. (2003) and Ford & Rasio (2008) show that when the planet masses are unequal the fraction of planet collisions relative to ejections is reduced and the eccentricities of the planets surviving after ejections are lower, resulting in a better match to the observed eccentricity distribution.

The latter experiments also show that the ratio of ejections to planet-planet collisions increases monotonically with a/R_p in the range $(0.5 - 2)$ (AU/R_J), where a is the semi-major axis, R_p is radius of the planet, and R_J is the radius of Jupiter. This behavior is related to the ratio θ of the escape velocity at the surface of the planet to the circular velocity of the planet:

$$\begin{aligned} \theta^2 &\equiv \left(\frac{2GM_p}{R_p} \right) \left(\frac{a}{GM_\star} \right) \\ &\approx \left(\frac{M_p}{M_J} \right) \left(\frac{M_\odot}{M_\star} \right) \left(\frac{R_J}{R_p} \right) \left(\frac{a}{0.25 \text{ AU}} \right), \end{aligned} \quad (1)$$

for $\theta \gg 1$ the planetary radius is so small that close encounters mostly lead to ejections relative to collisions, while for $\theta < 1$ collisions will be more frequent. Our definition of θ^2 differs from the so-called Safronov number because it uses the circular velocity of the planet instead of the relative velocity between planets.

Extrapolating the results by Ford et al. (2001) or Ford & Rasio (2008) to smaller orbital separations suggests that planet-planet collisions should happen even more frequently relative to ejections. However, this conclusion is sensitive to the particular initial conditions of these simulations. In particular, these authors initialize the orbital integrations with:

1. small relative orbital separations so the systems are Hill unstable,
2. nearly circular and coplanar orbital configurations,
3. and two planets.

With these initial conditions, the planets have small relative velocities (compared to their circular velocities) during the first close approaches, so gravitational focusing can significantly enhance the rate of collisions. Additionally, the simulations by Veras & Mustill (2013) show that

two-planet systems in Hill stable configurations can still be Lagrange unstable over sufficiently long timescales (at least $\sim 10^5$ orbits of the inner planet for two Jupiter-mass planets). Such systems contribute as an extra source of ejections and collisions with the star, while avoiding planet-planet collisions.

Simulations with more than two planets can become Hill unstable for larger initial separations between planets than in the two-planet case (e.g., Lin & Ida 1997; Levison et al. 1998; Papaloizou & Terquem 2001; Marzari & Weidenschilling 2002). This has the immediate consequence that close encounters for these larger separations happen after the planets have attained significant eccentricities, allowing close encounters to occur typically at higher relative velocities compared to the two-planet simulations, reducing the overproduction of collisions due to gravitational focusing.

These simulations show that the timescale for instability (time to the first orbit crossing) grows exponentially with the initial separation in units of the mutual Hill radii defined in Equation (3) (e.g., Chambers et al. 1996; Smith & Lissauer 2009). Once the eccentricities have grown, the number of planets gradually shrinks due to collisions between planets, planetary ejections, and collisions with the star, relaxing to a state in which three or fewer planets persist in eccentric orbits (Jurić & Tremaine 2008).

We extend previous studies by focusing on the dynamical evolution of systems of close-in planets ($0.05 \text{ AU} < a < 0.15 \text{ AU}$). We survey the parameter space of simulations with two and three planets to address whether planet-planet scattering can produce eccentricities and inclinations that are as large as those of the observed exoplanets. Recall that our goal is to test the scenario in which scattering takes place after the planets have migrated to (or formed at) small separations with small eccentricities and inclinations.

2. SIMULATIONS

We run N -body simulations of the evolution of the orbits of giant planets orbiting a solar-type star. In most simulations, the planets are assumed to have a Jupiter mass and radius. Planet-star and planet-planet collisions are assumed to result in momentum-conserving mergers with no fragmentation. Collisions are assumed to happen when the distance between two planets (or planet and star) becomes less than the sum of their physical radii. Since we consider planet-planet collisions, the problem at hand is not scale free, i.e., the results depend on the ratio a/R_p .

We start by studying simulations with two planets ($N_{pl} = 2$) because these have been the subject of extensive previous work and because understanding this simple case facilitates the analysis of simulations with more planets (e.g., Ford et al. 2001; Ford & Rasio 2008). However, two-planet systems have certain special features that are not found in systems with more than two planets. In particular, collisions can only happen if the planets initially lie inside the well-defined and narrow Hill unstable region (see discussion in §1). We also perform simulations with $N_{pl} = 3$, which are not subject to the latter restriction because systems can become Hill unstable for arbitrarily large initial separations between planets (e.g., Marzari & Weidenschilling 2002).

TABLE 1
SUMMARY OF SIMULATED SYSTEMS AND OUTCOMES

TWO-PLANET SIMULATIONS																	
Name	K	t_{\max} [yr]	σ_e^a	a [AU]	β	N_{sys}	2 pl.	C	E	S	E+S						
<i>2pl-fiducial</i>	2	10^6	0.01	0.05-0.15	1	1,000	792	184	11	7	6						
<i>2pl-K</i>	3	10^6	0.1	0.05-0.15	1	500	296	118	34	30	22						
<i>2pl-mass</i>	2	10^6	0.01	0.05-0.15	1/3	1,000	787	194	13	6	0						
THREE-PLANET SIMULATIONS																	
Name	K	t_{\max} [yr]	σ_x	a [AU]	N_{sys}	3 pl.	C	E	S	2C	2E	2S	C+E	C+S	E+S	C+E+S	2E+S
<i>3pl-fiducial</i>	3	10^6	0.01	0.05-0.15	1,000	255	692	3	0	0	0	1	21	10	3	15	0
<i>3pl-K</i>	4	10^7	0.01	0.05-0.15	500	83	367	0	0	24	0	2	12	8	1	3	0
<i>3pl-σ</i>	3	10^7	0.1	0.05-0.15	500	0	364	6	0	7	2	0	70	38	0	13	0
<i>3pl-a1</i>	3	5×10^6	0.01	0.15-0.45	500	124	303	13	3	0	0	3	9	29	11	6	0
<i>3pl-a2</i>	3	3×10^8	0.01	2.5-7.5	500	102	74	158	20	0	15	38	2	4	84	0	3

^a σ_i is kept constant and equal to 0.01 in all two-planet simulations.

Note: 2 pl. (3 pl.) means that two (three) planets remain in stable orbits for a time t_{\max} . C, E, and S stand for planet-planet collisions, planet ejections ($a > 10^3$ AU), and planet collisions with the star, respectively. 2C means that two planet collisions occur, while C+E means one collision and one ejection (not necessarily in that order), and so on.

The stellar mass is Solar and the planet masses are that of Jupiter, except for *2pl-mass* where we use $\beta = 1/3$ and $M_1 + M_2 = 2M_J$.

All the planets in the simulations have radius $R_i = R_J$.

We do not consider simulations with $N_{pl} > 3$. However, the simulations by Jurić & Tremaine (2008) with $N_{pl} > 3$ almost always end up with 2–3 surviving planets after ejections and collisions of other planets in the system. Then, as argued by Chatterjee et al. (2008), given the chaotic behavior of these systems, little memory of the initial number of planets or initial conditions will remain in the surviving planets. Therefore, it is plausible that the final state of systems initially with $N_{pl} > 3$ will be similar to that of systems with $N_{pl} = 3$.

Even though tidal dissipation can be important for planets that approach the host star within a few stellar radii, we ignore its effect. We justify this choice because we are interested in studying the maximum efficiency with which planet-planet scattering can produce high eccentricities and inclinations, and tides will only decrease this efficiency.

2.1. The code

We use the publicly available integration packages of MERCURY6.2 (Chambers 1999). In most simulations, we use MERCURY’s Bulirsch-Stoer (BS) integration algorithm; we justify this choice because we are mostly interested on the evolution of dynamically active systems, where planets experience close encounters, and the BS algorithm handles close encounters better than the other integration algorithms in MERCURY. We carry out integrations for up to $\sim 10^8$ orbits of the inner planet with an accuracy parameter $\epsilon = 10^{-12}$. In one set of simulations (*3pl-K*), we integrate up to $\sim 10^9$ orbits of the inner planet using MERCURY’s Hybrid integrator package, which integrates orbits symplectically, switching to the BS scheme when two planets have a close approach (defined to be closer than three Hill radii, as recommended by Duncan et al. 1998). In *3pl-K* we set the initial time step to be 0.5 days.

2.2. Initial conditions

We assume that the initial distributions in inclinations and eccentricities follow a Rayleigh law

$$dp = \frac{x dx}{\sigma_x^2} \exp\left(-\frac{1}{2}x^2/\sigma_x^2\right), \quad (2)$$

where $x = e$ or i and σ_x is an input parameter that is related to the mean, rms, and median eccentricity or inclination by $\langle x \rangle = \sqrt{\pi/2}\sigma_x = 1.253\sigma_x$, $\langle x^2 \rangle^{1/2} = \sqrt{2}\sigma_x = 1.414\sigma_x$, and $1.177\sigma_x$, respectively.

We measure the inclinations relative to the total angular vector of the planets in the initial configuration.

We choose the log of the semi-major axis to be uniformly distributed in a defined range. Labeling the planets by subscripts i in order of increasing semi-major axis, we impose a minimum initial spacing of the orbits given by

$$\Delta a_{i,i+1} \equiv a_{i+1} - a_i > K R_{H,i,i+1}, \text{ where} \\ R_{H,i,i+1} = \left(\frac{M_i + M_{i+1}}{3M_\star}\right)^{1/3} \frac{a_i + a_{i+1}}{2}, \quad (3)$$

and $R_{H,i,i+1}$ is the mutual Hill radius of planets with masses M_i and M_{i+1} .

The initial spacing between orbits mainly changes the timescale of onset of dynamical instability (e.g., Chambers et al. 1996). Our choice of K in Equation (3) is empirically guided by the fact that we would like to avoid very closely-packed systems that evolve on very short timescales, but still have a significant fraction of systems that become unstable after $\lesssim 10^8$ orbits of the innermost planet.

In most two-planet simulations we use $K = 2$. The Hill stability region for circular orbits to the lowest order in the mass ratios M_i/M_\star with $i = 1, 2$ is $\Delta a_{1,2} > 2\sqrt{3}a_1[(M_1 + M_2)/(3M_\star)]^{1/3}$ (Gladman 1993). This expression gives $K \simeq 3.46$ in Equation (3) but we use a slightly different value, $K \simeq 3.2$, because we include the first-order correction for Jupiter-mass planets. Thus, our choice of K ensures that there is a significant fraction of both Hill unstable and stable systems.

In most three-planet simulations we use $K = 3$. To obtain a crude estimate of the instability time, we rely on numerical experiments by Chatterjee et al. (2008) using a different initial spacing law $\Delta a_{i,i+1} = \tilde{K} R_{H,i,i+1}$ (i.e., the spacing is a fixed multiple of the Hill radius, rather than exceeding a multiple of the Hill radius). These authors show that for a distribution of planet masses in the

range $(0.4 - 4)M_J$ the median instability timescale⁴ can be fitted by the following expression

$$\log_{10}(t/\text{orbits}) = 0.021 + 0.03 \exp(1.1 \tilde{K}), \quad (4)$$

where the orbits are those of the innermost planet. Note that the instability timescale obtained for a given \tilde{K} is a lower limit to that obtained from our spacing law with $K = \tilde{K}$ in Equation (3). Thus, by setting $K = 3$ the minimum instability timescale is ~ 10 orbits and it rises rapidly to $\sim 10^7$ orbits for $\Delta a_{i,i+1}/R_{H,i,i+1} \simeq 5$.

In §4.1, we discuss how our results depend on K .

3. RESULTS

In Table 1, we summarize the input parameters, initial conditions, and outcomes of the different simulations. We have two fiducial simulations, *2pl-fiducial* and *3pl-fiducial*, corresponding to two- and three-planet systems. For these simulations we set the semi-major axis range to $0.05 - 0.15$ AU, $\sigma_x = 0.01$, and the maximum integration time to $t_{\text{max}} = 10^6$ years (or $\sim 10^8$ orbits for a planet at $a = 0.05$ AU). As discussed in §2.2, in *2pl-fiducial* we set $K = 2$, while in *3pl-fiducial* we use $K = 3$. In the rest of the simulations, we vary the parameters as indicated in Table 1. We define the mass ratio for the two-planet simulations as

$$\beta \equiv \min(M_1, M_2) / \max(M_1, M_2) \quad (5)$$

and fix $M_1 + M_2 = 2M_J$. All the planets in the three-planet simulations have Jupiter masses, while all planets in the two- and three-planet simulations have Jupiter radii.

We refer to *active* (*inactive*) systems as those in which the number of planets at the end of the simulation is less than (equal to) the number at the start. The number of planets is reduced by three different dynamical events: planet-planet collisions (C), planetary ejections (E), and planet collisions with the host star (S).

3.1. Outcomes from two-planet systems

In Figure 1, we show the results from our fiducial two-planet simulation *2pl-fiducial*. The possible outcomes are:

1. both planets survive on bound orbits until the end of the integration (“two planets”, red circles)
2. the two planets collide, producing one planet that remains on a bound orbit (“collisions”, blue circles)
3. one planet is ejected ($a > 1000$ AU) and the other remains on a bound orbit (“ejections”, green circles)
4. one planet collides with the star, leaving the other on a bound orbit (“collisions with star”, black circles)
5. one planet collides with the star and the other is ejected, leaving no planet in the systems.

⁴ We follow Chatterjee et al. (2008) in using the time to the first change in the semi-major axis of any planet by at least 10% as a measure of the dynamical instability growth timescale.

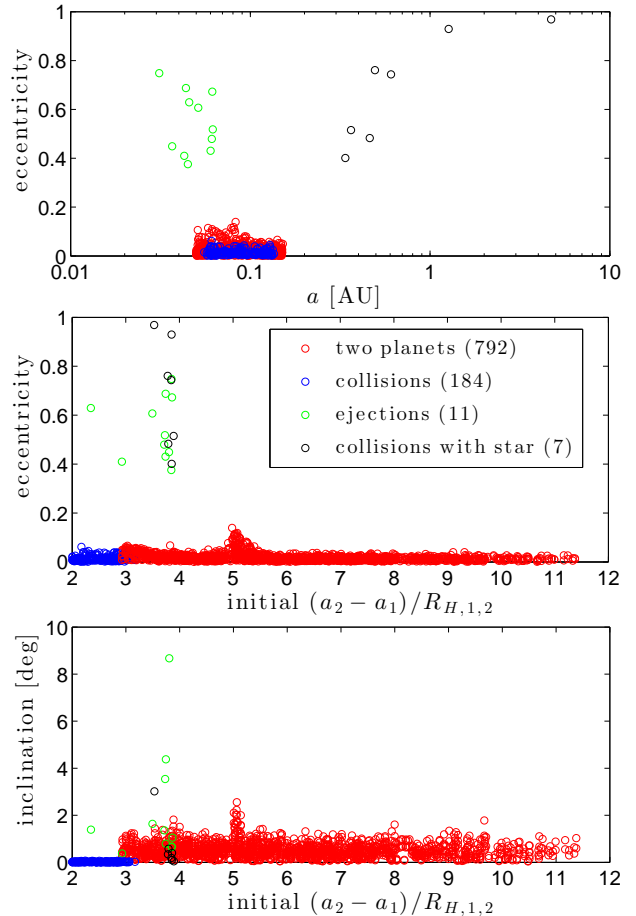


FIG. 1.— Final eccentricities and inclinations as a function of the final semi-major axis (upper panel) and initial spacing in units of Hill radii (middle and lower panels) for our fiducial simulation of two Jupiter-like planets *2pl-fiducial* (see Table 1). The colors label the different final outcomes. Each system was followed for 10^6 years. The log of the initial semi-major axis is drawn uniformly distributed in $a = 0.05 - 0.15$ AU with initial spacing given by $K = 2$ in Equation (3). The initial eccentricities and inclinations follow a Rayleigh distribution with $\sigma_x = 0.01$ (Eq. 2). Note that there are two red circles for each system in which both planets survive, so such systems might appear more common in these scatter plots than they actually are. Six additional systems are not plotted because one planet escaped and the second collided with the star, leaving none behind.

From Figure 1 and Table 1, the most common outcome is two planets in almost circular and coplanar orbits ($\approx 79\%$ of the systems). The initial separation of these systems is larger than $\approx 3.2R_{H,1,2}$, which corresponds to the Hill stability boundary for two Jupiter-mass planets (Gladman 1993). In these systems the final eccentricities are small (see second panel of Figure 1): the mean (median) eccentricity is 0.014 (0.02) and the eccentricity reaches a maximum of ≈ 0.14 for a small fraction of orbits with initial spacing of $\approx 5R_{H,1,2}$ corresponding to the 2 : 1 first-order mean-motion resonance. The feature seen around the resonance agrees with the prediction of Petrovich et al. (2013) for the time-averaged eccentricity distribution near this resonance.

The second most common outcome is planet-planet collisions ($\approx 18\%$). The initial separations of these systems are confined to $\Delta a_{1,2} \lesssim 3R_{H,1,2}$ and the collision product has a low-eccentricity orbit: the mean (median) eccentricity is only 0.014 (0.011). The small eccentrici-

ties of collision products is consistent with the results of similar simulations by Ford et al. (2001), which have a median eccentricity of ≈ 0.015 .

The least common outcome is planet ejections and collisions with the host star, each of which happens only $\approx 1\%$ of the time. The mean (median) eccentricity of the planets left after ejections and collision with host star is 0.54 (0.51) and 0.68 (0.74), respectively. Note that most of the ejections and collisions with the star ($\approx 89\%$) happen for initial separations $\Delta a_{1,2} \gtrsim 3R_{H,1,2}$ that are Hill stable, but become Lagrange unstable after $\sim 10^5$ orbits of the inner planet (Veras & Mustill 2013).

We observe that planet-planet collisions happen ≈ 11 and ≈ 14 times more frequently than ejections and collisions with the star, respectively. Given that planets in moderate to high eccentricities are only produced by planet ejections and collisions with the star, we conclude from these simulations that excitation of high eccentricities is very inefficient.

The inclinations are always small ($< 10^\circ$) in our simulations and the higher values ($\gtrsim 3^\circ$) are reached in systems where one planet is ejected. The extremely small inclinations (mean of $\approx 0.017^\circ$) in systems with collisions are easily understood as a result of angular momentum conservation during the collision of two planets.

We conclude from these experiments that planet-planet scattering in two-planet systems at $a \sim 0.1$ AU is almost never able to generate high eccentricities and inclinations. This is because the circular orbital velocity at these separations is bigger than the escape velocity of the planets ($\theta^2 = 0.2\text{--}0.6$ from Eq. 1) and, therefore, planet-planet collisions must happen more frequently than planet ejections.

3.2. Outcomes from three-planet systems

In Figure 2, we show the outcomes from our fiducial three-planet simulation *3pl-fiducial*. The different outcomes are summarized in Tables 1 and 2.

We note from Figure 2 and Table 1 that most systems ($\approx 69\%$) had one planet-planet collision, resulting in a final system having two planets. The second most common outcome ($\approx 25\%$) is a stable system in which all three planets survive for 10^6 years. The third most common channel ($\approx 3\%$) is a system having one collision with either one ejection ($\approx 2\%$) or one collision with the star ($\approx 1\%$), resulting in a final system with one planet. Then, we have one planet collision with a subsequent ejection and collision with the star ($\approx 1\%$), which leaves no planet in the system. Finally, we have $\lesssim 1\%$ systems with ejections and collisions with the star, or a combination of both not involving planet-planet collisions (i.e., $E \cup E+S \cup 2S$ in Table 1).

Other possible outcomes, not seen in *2pl-fiducial* are: S, 2C, 2E, 2E+S, and 2S+E.

The outcomes 3S, 2C+S, and C+2S are forbidden by angular momentum constraints, while 3E, 2C+E, and C+2E are forbidden by energy constraints.

From Figure 2 we see that the contribution to the active systems is not strongly confined to any particular initial spacing, as opposed to the simulations with two planets. Instead, the ratio of the number of active to inactive systems declines (non-red symbols to red symbols) gradually as the initial spacing increases. Equa-

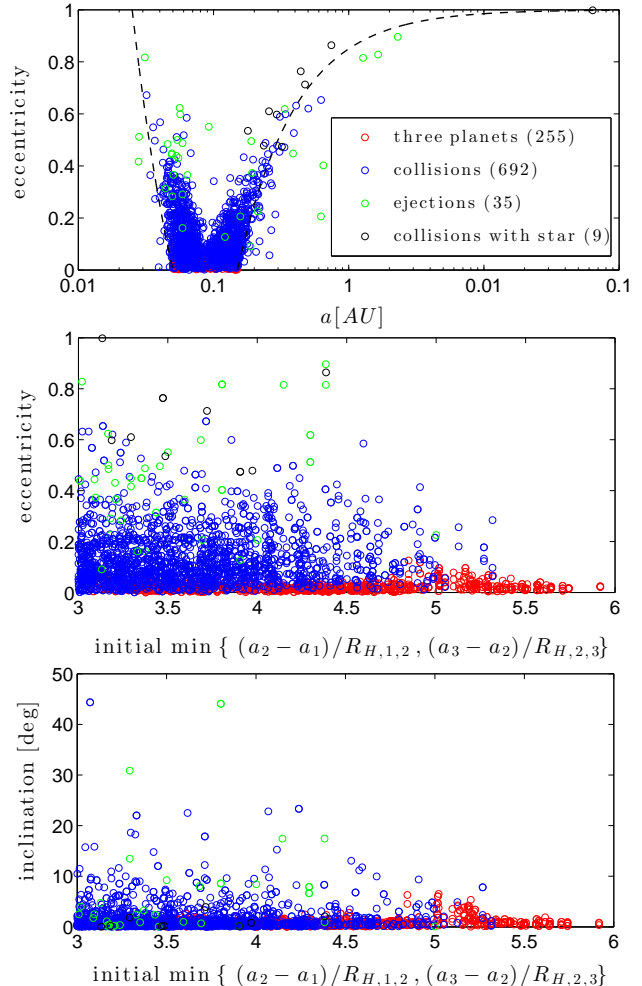


FIG. 2.— Final eccentricities and inclinations as a function of the final semi-major axis (upper panel) and initial spacing (middle and lower panels) for our fiducial simulation of three Jupiter-like planets *3pl-fiducial* (see Table 1). Each system was followed for 10^6 yr. The colors label the different final outcomes. The log of the initial semi-major axis is drawn uniformly distributed in $a = 0.05 - 0.15$ AU with minimum initial spacing given by $K = 3$ in Equation (3). The initial eccentricities and inclinations follow a Rayleigh distribution with $\sigma_x = 0.01$ (Eq. 2). The dashed lines in the upper panel show the curves $a(1+e) = 0.05$ AU and $a(1-e) = 0.15$ AU. Note that there are three red circles for each system in which all three planets survive, so such systems might appear more common in these scatter plots than they actually are. Fifteen additional systems are not plotted because all three planets were lost.

tion (4) predicts that the instability timescale is equal to our integration time at $\Delta a_{i,i+1} \approx 5R_{H,i,i+1}$, which is consistent with the observation that almost all of the systems with larger initial separations are inactive. To address how the initial spacing might affect our results, in §4.1 we perform a longer-term set of simulations with $\Delta a_{i,i+1} > 4R_{H,i,i+1}$.

The ratio of the number of planet-planet collisions to the number of ejections and collisions with the star increases from ≈ 6 in the two-planet simulation to ≈ 10 in the three-planet case. The prevalence of collisions over ejections or collisions with the star is consistent with similar three-planet simulations by Johansen et al. (2012).

Recall that in the two-planet simulations the ejections and collisions with the star happen predominantly

TABLE 2
ECCENTRICITIES AND INCLINATIONS FROM THE FIDUCIAL
THREE-PLANET SIMULATION

Outcome	Number of systems	eccentricity mean-median	inc. [deg] mean-median
3 pl	255	0.02 - 0.017	0.81 - 0.66
C	692	0.12 - 0.094	1.5 - 0.62
C+E	21	0.37 - 0.37	1.6 - 0.9
C+S	9	0.67 - 0.61	1.0 - 0.2
E	3	0.66 - 0.81	18 - 11
E+S \cup 2S	5	0.53 - 0.48	8.0 - 8.4
Total	985	0.096 - 0.052	1.3 - 0.65

for an initial spacing larger than $\Delta a_{1,2} \gtrsim 3.2R_{H,1,2}$, while planet-planet collisions are all confined to $\Delta a_{1,2} < 3.2R_{H,1,2}$. In contrast, in three-planet systems the different outcomes in active systems are not confined to any particular range of initial spacing (middle panel of Figure 2).

From Table 2 the mean (median) eccentricity for systems that had one planet-planet collision and no other events (category C; blue circles in Figure 2) is 0.12 (0.094). These values are larger than the mean eccentricity of 0.014 that results from collisions in the two-planet simulations. The category C systems have a characteristic fork-like eccentricity distribution. This distribution roughly agrees with the condition that the collision product has to pass through a region that was initially populated by planets: the interval between $a(1-e)$ and $a(1+e)$ must intersect $[0.05, 0.15]$ AU, as indicated with dashed lines in the upper panel of Figure 2.

High eccentricities ($e > 0.4$) are mainly reached in systems that had either ejections or collisions with the star, but the fraction of these systems is too small ($\lesssim 4\%$) to make an important contribution to the eccentricity distribution. By restricting the sample to the active systems, we find that 77% (92%) of the planets have $e < 0.2$ ($e < 0.3$), while all the planets in inactive systems have $e < 0.13$.

The inclinations are very low in most systems: $\simeq 95\%$ and $\simeq 99\%$ of the systems have $i < 5^\circ$ and $i < 10^\circ$, respectively. From Table 2, the mean and median inclinations are 1.3° and 0.65° , respectively. The low inclinations arise because most of the active systems ($\approx 70\%$) experience planet-planet collisions, which produce low-inclination collision products as a result of angular momentum conservation during the collision of two planets with nearly the same initial orbital planes.

In conclusion, the three-planet simulations confirm the main result found in the two-planet case: planet-planet scattering from nearly circular and coplanar orbits at small semi-major axes almost never produces high eccentricities and inclinations, because planet collisions are the dominant outcome and these tend to produce merger products with nearly circular and coplanar orbits.

3.3. Eccentricity distribution

In Figure 3, we show the final eccentricity distribution for all the surviving planets in active systems in our fiducial two- and three-planet simulations (solid black lines in upper and lower panels, respectively). We ignore inactive systems because their relative contribution depends strongly on the initial conditions and integration

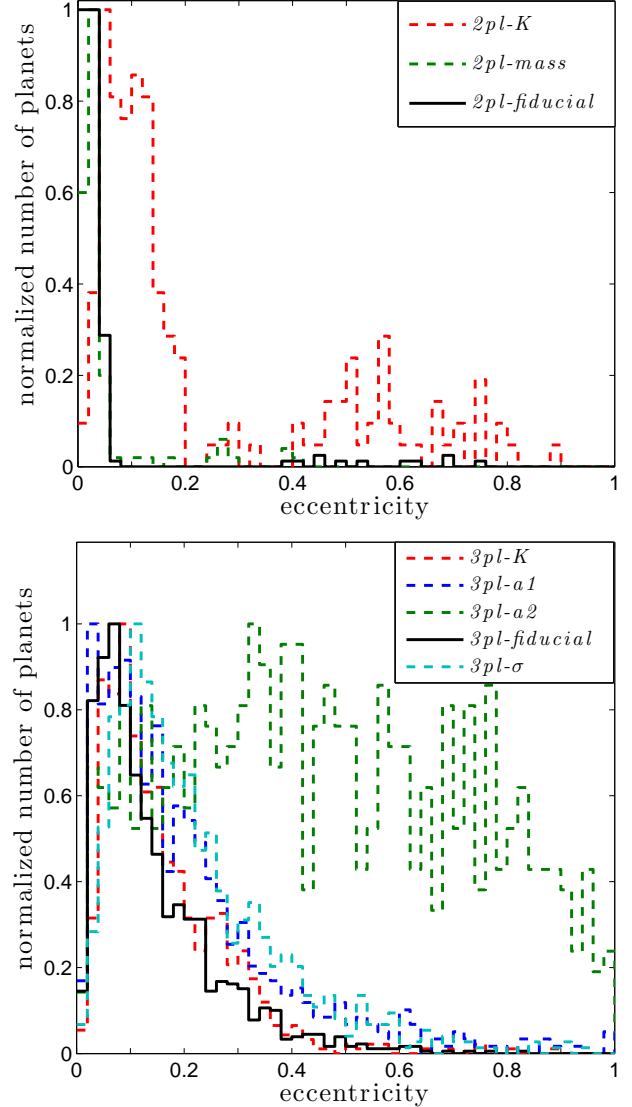


FIG. 3.— Final eccentricity distribution of all planets in the active systems for the simulations with two (upper panel) and three planets (lower panel). The labels indicate the name of the simulation (see Table 1). All histograms are normalized so the tallest bin has unit height. The bin width is 0.02.

time of the simulation. These systems, however, have even smaller eccentricities and inclinations and, therefore, make even stronger our conclusion that the production of high eccentricities and inclinations is inefficient.

The fiducial two-planet simulation has a strong peak at $e \lesssim 0.06$, which corresponds to the systems that had collisions, while the few systems that had either ejections or collisions with the star populate the distribution at $e > 0.35$. For the fiducial three-planet simulation, the distribution is strongly peaked at $e \lesssim 0.1$ due to the systems that had planet-planet collisions and is wider than in the two-planet case with collisions contributing to the distribution up to $e \sim 0.6$. The handful of planets with $e > 0.6$ are the result of ejections or collisions with the star.

In the two-planet simulations, collisions happen very early on in the simulation with $\approx 98\%$ of these events

taking place during the first 10^3 years. Before the collision planets experience an average of 1.5 close encounters (instances in which the relative distance between two planets is less than one Hill radius, not counting the last encounter in which planets merge). This suggests that collisions occur before repeated close encounters can excite the eccentricities. In this case planets would normally collide with low eccentricities, which would produce collision products in low eccentricity orbits⁵. Indeed, the typical eccentricity $e \lesssim 0.05$ seen in the collision products is consistent with analytical estimates of the eccentricities of collision products based on the assumption of low eccentricities for the pre-collision orbits (Ford et al. 2001; Goldreich & Sari 2003).

In contrast, in the three-planet simulations the collisions are more uniformly distributed in time. For instance, $\sim 30\%$ ($\sim 20\%$) of the collisions happen after 10^3 years (10^4 years). The number of close encounters before a collision is also larger in the three-planet simulations (average of 6.7 compared to 1.5 for the two-planet simulations), suggesting that the eccentricities of the pre-collision orbits are higher and thus that the eccentricity of the collision product should be larger, as observed. Consistently, the number of close encounters is correlated with the eccentricity after collisions (the correlation coefficient is ≈ 0.49) and almost all ($\approx 93\%$) of the planets with $e > 0.4$ had more than 10 close encounters before the collision.

4. DEPENDENCE ON INPUT PARAMETERS

We make an exploratory analysis of how our results depend on the properties of the two- and three-planet systems. Recall that the setup of each simulation and the outcomes are summarized in Table 1.

In Figure 3, we show the final eccentricity distribution for each simulation considering all the remaining planets in active systems. In Table 3, we show the mean and median eccentricities for the active, inactive, and all (active + inactive) systems in each simulation and the same for a sample of observed exoplanets in the same semi-major axis range.

4.1. Initial orbital spacing: K

We first test how our results depend on the initial spacing by running 500 two-planet simulations with $K = 3$, compared to $K = 2$ in the fiducial two-planet simulation (see description and outcomes of *2pl-K* in Table 1). This choice of K means that we exclude the initial spacings that give rise to most planet-planet collisions (see upper panel in Figure 1). In order to have a significant number of unstable systems we increase the initial eccentricities by setting $\sigma_e = 0.1$ in Equation (2), which would expand the Hill stability boundary by an approximate factor of $\sim (1 + 8/27(e_1^2 + e_2^2)/0.01)^{1/2}$, where $e_1, e_2 \lesssim 0.1$ are the initial eccentricities (Gladman 1993). This set-up has no direct theoretical motivation, but it might be regarded as the result of a previous dynamically active phase in the history of the system.

⁵ For planets colliding with low eccentricities, one can show that the mass-weighted eccentricity vector is conserved during the collision: $\mathbf{e}_c = (1 - \nu)\mathbf{e}_1 + \nu\mathbf{e}_2$, where $\nu = M_2/(M_1 + M_2)$ (e.g., Hénon & Petit 1986).

From Table 1, the ratio of the number of collisions to the number of ejections and collisions with the star decreases from ≈ 6 in the fiducial two-planet simulation to ≈ 1.1 . This result is expected from the larger initial eccentricities in *2pl-K*, which reduces the merger cross section. From Figure 3 and Table 3, we see that the eccentricity distribution broadens and the median eccentricity grows from 0.012 in the fiducial simulation to 0.12. This behavior is the result of two effects: the higher number of ejections and collisions with the star relative to planet-planet collisions (systems with $e > 0.2$ in Figure 3) and higher eccentricities after collisions (systems with $e < 0.2$). The latter effect is expected from the higher initial eccentricities and the larger number of close encounters before collisions (the average increases from 1.5 in the fiducial simulation to 12), because both effects promote higher eccentricities and, therefore, collisions at higher relative velocities.

Despite these differences, the main conclusion of this paper still holds: planet-planet scattering cannot efficiently excite eccentricities and inclinations at small semi-major axes. Although the mean and median eccentricities of 0.27 and 0.12 of the active systems in *2pl-K* bracket the analogous quantities in the observed exoplanet sample (0.19 and 0.17), (i) the initial conditions of the simulation already had mean and median eccentricities of 0.125 and 0.117 so only part of the final eccentricity is due to excitation; (ii) realistic ensembles would contain many inactive systems, in which almost no eccentricity excitation occurs; (iii) in systems with $K = 3$ and zero initial eccentricity almost all of the systems are inactive.

The mean (median) inclination in active systems is only 0.83° (0.04°). We note that *2pl-K* starts with a wide eccentricity distribution (mean eccentricity of 0.125) close to the dispersion-dominated regime ($|\mathbf{e}_1 - \mathbf{e}_2| \gtrsim [(M_1 + M_2)/M_\star]^{1/3} = 0.126$, where \mathbf{e}_i is the eccentricity vector of planet $i = 1, 2$) and small inclinations well in the shear-dominated regime (relative inclinations $\ll [(M_1 + M_2)/M_\star]^{1/3}$). Such systems can excite eccentricities much more efficiently than the inclinations (Ida & Makino 1992; Rafikov & Slepian 2010), which is consistent with the simulations where the final inclinations are much smaller than the final eccentricities.

We carry out a similar experiment for the three-planet systems, increasing K from 3 to 4 and increasing the integration time from 10^6 to 10^7 years (see simulation *3pl-K* in Table 1). We integrate 500 systems, using the Hybrid algorithm to speed up the integrations as described in §2.1.

From Table 1, the ratio of the number of collisions to the number of ejections and collisions with the star is ≈ 13 , similar to that from the fiducial three-planet simulation of ≈ 10 . This result suggests that this ratio is independent of K in the three-planet systems. This conclusion is not unexpected since the planet-planet collisions in the three-planet simulations come from a wide range of initial separations (middle panel of Figure 2).

An outcome that was not present in the fiducial simulation is two successive planet-planet collisions (2C in Table 1) leaving a single planet with $3M_J$. This outcome has a branching ratio of 2% in the simulation *3pl-K*, and appears to require a minimum orbital spacing

TABLE 3
MEAN AND MEDIAN ECCENTRICITIES OF SIMULATED SYSTEMS AND SAMPLE OF OBSERVED EXOPLANETS.

Simulation	ecc. active mean - median	ecc. inactive mean - median	ecc. all mean - median	ecc. observed mean-median
<i>2pl-fiducial</i>	0.067 - 0.012	0.019 - 0.015	0.024 - 0.014	0.19 - 0.17
<i>2pl-K</i>	0.27 - 0.12	0.10 - 0.11	0.15 - 0.10	0.19 - 0.17
<i>2pl-mass</i>	0.034 - 0.015	0.020 - 0.015	0.022 - 0.015	0.19 - 0.17
<i>3pl-fiducial</i>	0.13 - 0.098	0.020 - 0.017	0.096 - 0.052	0.19 - 0.17
<i>3pl-K</i>	0.15 - 0.11	0.017 - 0.015	0.12 - 0.085	0.19 - 0.17
<i>3pl-σ</i>	0.21 - 0.16	—	0.21 - 0.16	0.19 - 0.17
<i>3pl-a1</i>	0.19 - 0.14	0.021 - 0.018	0.13 - 0.061	0.29 - 0.18
<i>3pl-a2</i>	0.45 - 0.44	0.023 - 0.018	0.31 - 0.25	0.27 - 0.23

Note: we select a sample of exoplanets from www.exoplanet.org as of November 2013 in which the planets have $M \sin(i) > 0.1 M_J$ and semi-major axis within the range of each simulation. We exclude the planets with $a < 0.07$ AU to avoid the excess of planets with small eccentricities likely due to tidal circularization.

For reference, the number of inactive systems is given in Table 2 in the columns 2 pl. and 3 pl. for the two- and three-planet simulations. Note that *3pl-σ* has no inactive systems.

of $\approx 4.5 R_{H,i,i+1}$, where the fiducial simulation contains only a small fraction of active systems because of its shorter integration time.

From Figure 3, the eccentricity distribution in *3pl-K* is slightly broader than the fiducial three-planet simulation. From Table 3, the small increase in mean and median eccentricity still falls short compared to the observed exoplanets. Likewise, the mean (median) inclination is only 2.0° (1.0°).

In summary, the effect of increasing the initial spacing is to increase the final eccentricity of the active systems, while decreasing the fraction of active systems. The combined effect of these two changes is not strong enough to alter our conclusion that eccentricity and inclination excitation is inefficient at small semi-major axes.

4.2. Initial semi-major axis: a

From Equation (1), we observe that for a fixed planet to star mass ratio the physical parameter that governs the relative branching ratios for ejections (or collisions with the star) and collisions is a/R_p . Given that most giant planets have radii close to R_J , one expects that the branching ratios are mostly determined by the semi-major axis.

In the simulations *3pl-a1* and *3pl-a2*, we place three planets with the log of the semi-major axis uniformly distributed in the range $a = 0.15 - 0.45$ AU and $a = 2.5 - 7.5$ AU, which are larger than the semi-major axis range in our fiducial simulation by factors of 3 and 50.

We first describe our results for *3pl-a2*, the simulation with the largest semi-major axes. From Table 1, the ratio of the number of collisions to the number of ejections and collisions with the star decreases dramatically from ≈ 10 in the fiducial three-planet simulation to ≈ 0.17 . This sharp decrease is expected since the planets in *3pl-a2* have $\theta^2 = 10 - 30$ compared to $\theta^2 = 0.2 - 0.6$ in the fiducial simulation.

From Figure 3, the eccentricity distribution in active systems broadens significantly relative to the fiducial three-planet simulation. The median eccentricity of the active systems rises from 0.098 in the fiducial simulation to 0.44 in *3pl-a2* while the median eccentricity of all the systems is 0.25, compared to the observed median eccentricity of 0.23 in this semi-major axis range.

Likewise, the distribution of inclinations in *3pl-a2* broadens significantly and the mean (median) inclination in active systems becomes 15° (10°).

We next turn to the simulation *3pl-a1* in which the planets have $\theta^2 = 0.6 - 1.8$. From Table 1, the ratio of the number of collisions to the number of ejections and collisions with the star decreases from ≈ 10 in the fiducial three-planet simulation to ≈ 5.6 . This reduction in the relative number of collisions broadens the eccentricity distribution (Figure 3): the median eccentricity of the active systems increases from 0.098 in the fiducial simulation to 0.14 in *3pl-a1*. These higher eccentricities in *3pl-a1* are, however, still smaller than the measured eccentricities (Table 3). Finally, the mean (median) inclination is 3.2° (1.0°), slightly larger than the fiducial three-planet simulation (Table 2).

In conclusion, placing the planets in larger semi-major axis enhances the efficiency to produce ejections and collisions with the star and, therefore, the outcomes of active systems have higher eccentricity and inclination orbits. Our simulation *3pl-a2* shows that scattering at $a = 2.5 - 7.5$ AU produces eccentricities in the active systems that are larger than those measured from the observed exoplanets in this semi-major axis range, so the results could be consistent with the observations if a significant fraction of the observed systems are inactive. In contrast, the simulations with planets at $a < 0.45$ AU (*3pl-fiducial* and *3pl-a1*) predict eccentricities that are smaller than those seen in our exoplanet sample, even if we restrict ourselves to active systems, which is mainly due to the prevalence of planet collisions. We remark that the evolution of the different branching ratios as a function of a/R_p has been previously studied by Ford et al. (2001) in simulations with two planets and our results point in the same direction: the number of collisions per ejections decreases with increasing a/R_p .

4.3. Planet mass ratio: β

As shown by Ford et al. (2003) and Ford & Rasio (2008), the ratio of collisions to ejections decreases as the mass ratio β in Equation (5) shrinks.

To test how sensitive our results are to the mass ratio, we ran 1,000 simulations similar to the fiducial two-planet simulation, changing the mass ratio from $\beta = 1$

to $\beta = 1/3$ (simulation *2pl-mass* in Table 1). We initialize the system with two planets with masses $0.5M_J$ and $1.5M_J$ and randomly pick one planet to have the smaller semi-major axis. We fix the planets' radii to that of Jupiter⁶.

From Table 1, the ratio of the number of systems that have planet collisions to the number of systems with ejections and collisions with the star increases from 6 for the fiducial simulation to 10 for *2pl-mass*, although this change is not significant given the Poisson errors in the simulations. We do not see the reduction in the number of collisions observed in the simulations by Ford et al. (2003). This difference might be due to the fact that most of the ejections and collisions with the star happen in systems that are Hill stable, which are excluded in the simulations by Ford et al. (2003).

If a planet is ejected, it is always the lighter one, while the median eccentricity of the planet left is 0.26. This median eccentricity falls within the range $\sim 0.2 - 0.4$ found by Ford & Rasio (2008) for the same mass ratio and is lower than that observed in the fiducial two-equal-mass-planet simulation.

From Table 3, the mean and median eccentricities of *2pl-mass* are smaller than those of the observed exoplanets, as is the case for the fiducial two-planet simulation. The mean (median) inclinations are 0.57° (1.1°).

In summary, the overall effect of having unequal-mass planets is to produce lower eccentricities after ejections (at least for $\beta = 1/3$). Changing β to more extreme values would not change our main conclusion because, even if the number of collisions per ejection decreases, Ford & Rasio (2008) showed that the eccentricity of the surviving planet after the ejection would decrease with decreasing β (for reference Ford & Rasio 2008 find $e \lesssim 0.2$ for $\beta = 1/9$). Likewise, the final inclinations after ejections are also limited as one decreases β (e.g., Timpe et al. 2013). In conclusion, the excitation of eccentricities and inclinations is inefficient even if the mass ratio departs from unity.

4.4. Initial eccentricity and inclination: σ_x

In *3pl- σ* we initialized the orbits with a broader eccentricity and inclination distribution ($\sigma_i = \sigma_e = 0.1$ in Eq. [2]; mean of 0.125) compared to our fiducial three-planet simulation ($\sigma_i = \sigma_e = 0.01$).

From Table 1, the ratio of the number of collisions to the number of ejections and collisions with the star decreases from ≈ 13 in the fiducial three-planet simulation to ≈ 3.2 . Similar to the simulation *2pl-K* discussed in §4.1, this is expected from the larger initial eccentricities and inclinations in *3pl- σ* , which reduces the merger cross section. From Figure 3 and Table 3, we see that the eccentricity distribution in active systems broadens and the median eccentricity grows from 0.098 in the fiducial simulation to 0.16.

The mean and median eccentricities of 0.21 and 0.16 of the active systems in *3pl- σ* bracket the analogous quantities in the observed exoplanet sample (0.19 and 0.17). However, as discussed in §4.1 for *2pl-K*, only part of the

final eccentricity is due to excitation because the initial conditions of the simulation already had mean and median eccentricities of 0.125 and 0.117. In addition, realistic ensembles would contain many inactive systems, in which almost no eccentricity excitation occurs. Thus, our conclusion that planet-planet scattering cannot efficiently excite eccentricities and inclinations at small semi-major axes should still hold.

The distribution of inclinations in *3pl- σ* also broadens significantly relative to the fiducial simulation and the mean (median) inclination in active systems becomes 6° (4.5°).

5. DISCUSSION

The main result from our orbit integrations is simple: at small semi-major axes, gravitational interactions between planets in unstable systems mostly lead to collisions rather than to excitation of highly eccentric and inclined planetary orbits.

Collisions are more common than ejections or collisions with the star because the orbital velocities at small separations are typically larger than the escape velocity of giant planets (see Eq. 1, for reference). A similar conclusion is reached in the numerical study by Johansen et al. (2012). Moreover, planet-planet collisions from low-eccentricity, low-inclination orbits typically produce collision products that occupy orbits with even lower eccentricity and inclination. The low-inclination orbits are easily understood as a result of angular momentum conservation during the collision of two planets with nearly the same initial orbital planes.

Consequently, our simulations with two or three planets initially in low-eccentricity orbits at $a = 0.05 - 0.15$ AU (i.e., excluding *2pl-K* and *3pl- σ*) predict mean (median) final eccentricities for the active systems that are $\simeq 1.3 - 8$ ($\simeq 1.5 - 14$) times smaller than those observed in the exoplanets in a similar semi-major axis range (Table 3). Moreover, if we include planets from the inactive systems the mean and median eccentricities will be even smaller. For instance, the mean (median) eccentricities for all (active + inactive) planets in each simulation is $\simeq 1.6 - 9$ ($\simeq 2 - 12$) times smaller than the observed values.

The previous result holds even for the simulations with three Jupiter-like planets initially at semi-major axes as large as $a = 0.15 - 0.45$ AU because the mean (median) eccentricities of planets in active systems is 1.5 (1.3) times smaller than those observed in the data. This result breaks down when placing the planets at $a = 2.5 - 7.5$ AU because these simulations predict mean and median eccentricities in active systems that are larger by a factor of $\simeq 2$ than those observed in the data. However, this simulation can be made consistent with the data by adding a significant fraction of inactive systems. The eccentricities in the simulations above are larger than those in the fiducial simulation because of the dramatic decrease in the relative number of planet collisions in active systems as we increase the semi-major axis (or θ^2 in Eq. 1).

In *2pl-K* and *3pl- σ* we initialized the orbits with a broad eccentricity distribution (mean of 0.125) that might result from a previous dynamically active phase when the gas disk is present (Libert & Tsiganis 2009; Lega et al. 2013). As discussed in §4.1 and §4.4, these

⁶ This mass-radius relation is also equivalent to fixing the planets' escape velocity to that of Jupiter (i.e., $M/R = M_J/R_J$) because it results in the same condition for collisions for this particular value of the mass ratio β : distance between planets $< 2R_J$.

simulations starts close to the dispersion-dominated regime, in contrast to the rest of the simulations which are well in the shear-dominated regime (Hénon & Petit 1986). We observe, however, that even in these more extreme conditions planet-planet collisions dominate the branching ratios, limiting the eccentricity excitation. By considering that realistic ensembles would contain a mixture of active and inactive systems our conclusion that scattering at small semi-major axis is unable to explain the observations can still hold.

Our simulations suggest that in order to have final eccentricities that are as high as in the observations the initial eccentricities had to be previously excited to $e \gtrsim 0.1$. In principle, eccentricity excitation could be produced by effects that we have ignored in our simulations. For instance, a combination of tides with the host star, secular precession effects, and secular interactions with a relatively distant companion can lead to eccentricity excitation of a close-in planet (Wu & Goldreich 2002; Correia et al. 2012). However, this mechanism requires a companion in particular orbital configurations and specific values of tidal dissipation that might not be present in the bulk of planetary systems (Correia et al. 2012).

Another possibility is that during the assembly of our initial systems, the planets had crossed high-order mean motion resonances (e.g., 3 : 1, 4 : 1, and so on) that could lead to eccentricity and inclination excitation (Libert & Tsiganis 2009). This possibility is speculative and would require convergent migration of planets in which case planet-planet scattering is likely to have occurred before the planets reach semi-major axis that are as small as in our simulations. Also, the gravitational interactions with the protoplanetary disk could potentially excite eccentricities during the assembly of our initial conditions (Goldreich & Sari 2003; Tsang et al. 2014).

We expect that simulations with more than three planets would present a similar behavior as our three-planet experiments. Our expectation is guided by the experiments of Jurić & Tremaine (2008) who find that regardless of the initial conditions and initial number of planets, the systems almost always reach a point in which there are three planets. There might be two shortcomings with this reasoning. First, having many planets in active systems can leave the three planets in orbits with significant eccentricities, which reduces the merger cross section. Second, after several merger events the planets can increase their masses and, therefore, their escape velocities. Both effect can reduce the rate of collisions.

Tidal dissipation with the host star should significantly affect the long-term dynamical evolution of close-in planets. Matsumura et al. (2008) suggest that indeed some of the observed eccentric close-in planets are in the process of getting tidally circularized. We have, however, ignored the effect of tides in our calculations. We expect that the main effect would be to damp the eccentricities and given that we are mostly interested in determining the maximum efficiency of planet-planet scattering at producing high eccentricities, the effect of tides would only make our conclusion stronger.

5.1. Planet-planet scattering and migration

From our main result, we can draw the following straightforward conclusion: if planet-planet scattering is responsible for the highly eccentric and inclined plan-

etary orbits seen in many exoplanets with small semi-major axes, then the scattering must have occurred at much larger orbital separations.

Interestingly, this conclusion links the migration mechanism or assembly process with the excitation of eccentricities and inclinations. For instance, we can rule out the scenario in which planets undergo disk-driven migration to small radii with no eccentricity and inclination excitation. We can also rule out the scenario in which planets are assembled in close-in nearly circular and planar orbits, for instance as a result of a binary merger, as proposed by Martin et al. (2011).

Our results would support a scenario in which planet-planet scattering excites the eccentricities and inclinations either before or early on in the migration process, so long as these are not damped during migration.

In this context, Moorhead & Adams (2005) did a parametric study of type II migration coupled with planet-planet scattering and found that in order to explain the observations disk migration requires that $|\dot{e}/e| \lesssim 3 |\dot{a}/a|$, where $\dot{e} < 0$ ($\dot{a} < 0$) is the time-derivative of the eccentricity (semi-major axis). For eccentricity damping more efficient than this limit, planets end-up with eccentricities that are too small by the time they reach $a \sim 0.1$ AU. On the other hand, observational constraints from planet pairs thought to be trapped in orbital resonances during convergent migration (Lee & Peale 2002; Goldreich & Schlichting 2013), as well as hydrodynamic simulations⁷ (e.g., Cresswell et al. 2006; Bitsch et al. 2011; Kley & Nelson 2012) seem to indicate that $|\dot{e}/e| \gg |\dot{a}/a|$. This would mean that eccentricity damping occurs much faster than migration, so even if scattering excites eccentricities early on during migration these eccentricities would be damped by the time the planet migrated to $a \sim 0.1$ AU. This might pose a problem for disk-driven migration scenarios. Direct hydrodynamic simulations coupled with the gravitational interaction between planets (Moeckel et al. 2008; Moeckel & Armitage 2012; Lega et al. 2013) or planet population models (Ida et al. 2013) might shed light on this issue.

These difficulties with disk migration are not present (or, at least, replaced with different difficulties) in models of the formation of Hot Jupiters through high-eccentricity migration. In these models, planets are scattered to high eccentricities and inclinations at large semi-major axes, and then migrate inwards through tidal dissipation by the host star. Numerical simulations have shown that this mechanism can produce close-in planets in highly eccentric and inclined orbits (e.g., Nagasawa et al. 2008; Beaugé & Nesvorný 2012).

6. SUMMARY

We carried out a large number of orbit integrations of close-in two- and three-planet systems ($0.05 \text{ AU} < a < 0.15 \text{ AU}$) and studied whether planet-planet scattering can excite high-eccentricity and high-inclination orbits. We show that this mechanism is almost never able to excite eccentricities larger than ~ 0.3 and inclinations larger than 10° , and the most likely outcome is typically $e \lesssim 0.1$ and $i \lesssim 5^\circ$.

⁷ Note, however, that hydrodynamic simulations show that for massive planets ($M > 5M_J$) disk-planet interaction can lead to eccentricity excitation (e.g., Bitsch et al. 2013; Dunhill et al. 2013).

This remarkably low efficiency of eccentricity and inclination excitation results from the prevalence of planet-planet collisions, which is an unavoidable outcome of unstable systems in regimes where the circular velocity exceeds the escape velocity from the planets.

We conclude that if planet-planet scattering is responsible for the highly eccentric and inclined planetary orbits seen in many exoplanets with small semi-major axes, then the scattering must have occurred at much larger orbital separations. This result constrains theories of planet formation by disk migration: the eccentricities and inclinations observed in extrasolar planets must be excited before or early in the migration process, and mi-

gration must shrink the semi-major axis by $\sim 1-2$ orders of magnitude without damping the eccentricity or inclination.

CP acknowledges support from the CONICYT Bicentennial Becas Chile fellowship. ST thanks Henk Spruit for the conversations that stimulated this paper, and the Max Planck Institute for Astrophysics, the Alexander von Humboldt Foundation, and the Miller Institute for Basic Research in Science, University of California Berkeley for support and hospitality. All simulations were carried out using computers supported by the Princeton Institute of Computational Science and Engineering.

REFERENCES

- Barnes, R., & Greenberg, R. 2006, *ApJ*, 647, L163
 Beaugé, C., & Nesvorný, D. 2012, *ApJ*, 751, 119
 Bitsch, B., Crida, A., Libert, A.S., & Lega, E. 2013, *A&A*, 555, A124
 Bitsch, B. & Kley, W. 2011, *A&A*, 530, A41
 Chambers, J. E. 1999, *MNRAS*, 304, 793
 Chambers J. E., Wetherill G. W., & Boss A. P., 1996, *Icarus*, 119, 261
 Chatterjee, S., Ford, E. B., Matsumura, S., & Rasio, F. A. 2008, *ApJ*, 686, 580
 Correia, A. C. M., Boué, G., & Laskar, J. 2012, *ApJL*, 744, L23
 Cresswell, P., Dirksen, G., Kley, W., & Nelson, R. P. 2007, *A&A*, 473, 329
 Deck, K. M., Payne, M., & Holman, M. J., 2013, *ApJ*, 774, 129
 Duncan, M. J., Levison, H. F., & Lee, M. H. 1998, *AJ*, 116, 2067
 Dunhill, A. C., Alexander, R. D., & Armitage, P. J. 2013, *MNRAS*, 428, 3072
 Fabrycky, D., & Tremaine, S. 2007, *ApJ*, 669, 1298
 Ford, E. B., Havlickova, M., & Rasio, F. A. 2001, *Icarus*, 150, 303
 Ford, E. B., & Rasio, F. A. 2008, *ApJ*, 686, 621
 Ford, E. B., Rasio, F. A., & Yu, K., 2003, in *ASP Conf. Ser. Vol 294, Scientific Frontiers in Research on Extrasolar Planets*. Astron. Soc. Pac., San Francisco, p. 181
 Gladman, B. 1993, *Icarus*, 106, 247
 Goldreich, P., & Sari, R. 2003, *ApJ*, 585, 1024
 Goldreich, P., & Schlichting, H. E. 2013, *AJ*, 147, 32
 Hénon, M., & Petit, J. M. 1986, *CeMec*, 38, 67
 Ida, S., Lin, D. N. C., & Nagasawa, M. 2013, *ApJ*, 775, 42
 Ida, S., & Makino, J. 1992, *Icarus*, 96, 107
 Johansen, A., Davies, M. B., Church, R. P., & Holmelin, V. 2012, *ApJ*, 758, 39
 Jurić, M., & Tremaine, S. 2008, *ApJ*, 686, 603
 Kley, W., & Nelson, R. P. 2012, *AARA*, 50, 211
 Lee, M. H., & Peale, S. J. 2002, *ApJ*, 567, 596
 Lega, E., Morbidelli, A., & Nesvorný, D. 2013, *MNRAS*, 431, 3494
 Levison, H.F., Lissauer, J. J., & Duncan, M. J. 1998, *AJ*, 116, 1998
 Libert, A.-S. & Tsiganis, K. 2009, *MNRAS*, 400, 1373
 Lin, D. N. C. & Ida, S. 1997, *ApJ*, 477, 781
 Martin, E. L., Spruit, H. C., & Tata, R. 2011, *A&A*, 535, A50
 Marzari, F. & Nelson, A. F. 2009, *ApJ*, 705, 1575
 Marzari, F. & Weidenschilling, S. J. 2002, *Icarus*, 156, 570
 Matsumura, S., Takeda, G., & Rasio, F.A. 2008, *ApJL*, 686, L29
 Moeckel, N., & Armitage, P. J. 2012, *MNRAS*, 419, 366
 Moeckel, N., Raymond, S. N., & Armitage, P. J. 2008, *ApJ*, 688, 1361
 Moorhead, A., & Adams, F. 2005, *Icar*, 178, 517
 Nagasawa, M., Ida, S., & Bessho, T. 2008, *ApJ*, 678, 1
 Naoz, S., Farr, W. M., Lithwick, Y., Rasio, F. A., & Teyssandier, J. 2011, *Natur*, 473, 187
 Ogilvie, G. I. & Lubow, S. H., 2003, *ApJ*, 587, 398
 Papaloizou, J. C. B., & Terquem, C. 2001, *MNRAS*, 325, 221
 Petrovich, C., Malhotra, R., & Tremaine, S. 2013, *ApJ*, 770, 24
 Rafikov, R. R., & Slepian, Z. S. 2010, *AJ*, 139, 565
 Rasio, F. A. & Ford, B. E., 1996, *Sci*, 274, 954
 Smith, A. W., & Lissauer, J. J. 2009, *Icar*, 201, 381
 Timpe, M., Barnes, R., Kopparapu, R., et al. 2013, *ApJ*, 146, 63
 Tsang, D., Turner, N. J., & Cumming, A. 2014, *ApJ*, 782, 113
 Veras, D., & Mustill, A. J. 2013, *MNRAS*, 434, L11
 Weidenschilling, S. J. & Marzari, F., 1996, *Natur*, 384, 619
 Wu, Y., & Goldreich, P. 2002, *ApJ*, 564, 1024
 Wu, Y. & Lithwick, Y. 2011, *ApJ*, 735, 109
 Wu, Y. & Murray, N. 2003, *ApJ*, 589, 605